

Static potential and local color fields in unquenched lattice QCD₃

Howard D. Trottier and Kit Yan Wong
*Simon Fraser University, Department of Physics,
 8888 University Drive, Burnaby BC V5A 1S6, Canada*

String breaking by dynamical quarks in three-dimensional lattice QCD is analyzed through measurements of the potential and the local color-electric field strength generated by a static quark-antiquark pair. Simulations were done for unquenched SU(2) color with two flavors of staggered light quarks. An improved gluon action was used, which allows simulations to be done on coarse lattices, providing an extremely efficient means to access the large quark separations and long propagation times at which string breaking occurs. The static sources were generated using Wilson loop operators, hence no light valence quarks are present in the resulting trial states. Results give unambiguous evidence of string breaking. First the static potential is shown to saturate at twice the heavy-light meson mass at large separations. Then it is demonstrated that the local color-electric field strength in the region between the heavy quarks tends towards vacuum values at large separations, the first time that this most graphic effect of quark vacuum polarization on the confining flux-tube has been realized in lattice QCD. Implications of these results for unquenched simulations of four-dimensional QCD are drawn.

I. INTRODUCTION

The string model is widely used in phenomenologies of quark confinement and hadronization. A basic system of interest in the string model consists of a heavy quark (Q) and antiquark (\bar{Q}) pair, which are assumed to be bound by a narrow tube of color flux. This model naturally gives rise to a linearly confining potential, if the tube has a cross-section that is approximately independent of the quark separation [1]. In fact simulations of quenched lattice QCD long ago demonstrated the formation of color-flux tubes having properties that are in accord with simple models.

In full QCD the confining $Q\bar{Q}$ string should not persist to arbitrarily large separations R , due to the effects of dynamical sea quarks. One expects that it becomes energetically favorable for a light quark (q) and antiquark (\bar{q}) to materialize from the Dirac sea at large R , and the light quarks should bind to the heavy quarks resulting in the formation of a pair of noninteracting color-neutral mesons. This phenomenon of hadronization, or string breaking, implies for instance that the potential $V(R)$ for a static $Q\bar{Q}$ pair should saturate at large separations,

$$\lim_{R \rightarrow \infty} V(R) = 2M_{Q\bar{q}}, \quad (1)$$

where $M_{Q\bar{q}}$ is the mass of the ground-state heavy-light meson.

Observation of Eq. (1) in an unquenched lattice QCD simulation provides the simplest criterion to demonstrate string breaking. A much more detailed probe of this basic phenomenon of hadronic physics would come from measurements of the local color fields $f_{\mu\nu}(x; R)$ as functions of position x in the region between the static valence quarks, for various values of R . The effects of dynamical quarks should be to suppress the fields in the region between the static sources, with the fields saturating at vacuum values in the limit of large R

$$\lim_{R \rightarrow \infty} f_{\mu\nu}(x; R) = 0, \quad (2)$$

for x outside a finite region surrounding each static valence quark, corresponding to the size of the $Q\bar{q}$ meson.

Despite considerable effort, however, it has proven to be very difficult to establish Eq. (1), and especially Eq. (2), in unquenched lattice QCD simulations [2, 3, 4]. The traditional computational strategy is to use Wilson loop operators in order to create trial states containing only static sources, with no valence light quarks. In that case Eqs. (1) and (2) provide unambiguous evidence of the effects of light quarks that “materialize” from the sea (one must take care to note however that Euclidean lattice simulations only provide an analogy to the real-time process of hadronization). The difficulty in making these measurements on the lattice is due in part to the exponential suppression of the correlators, reflecting the large energy of the state at large separations R , and the large propagation time T which is necessary in order to isolate the ground state of the system [5, 6, 7].

A convincing demonstration of the saturation of the unquenched $V(R)$ has only recently been achieved, thanks in part to the realization that improved actions can be used to do accurate simulations on lattices with coarse grids, where the computational effort can go into generating large ensembles of gauge-fields at the large length scales relevant to string breaking, rather than to generating short-distance modes that are not of interest here [5, 6]. Studies of the local color-fields are still more problematic than the static potential; the simplest definition of $f_{\mu\nu}(x; R)$ comes from the correlator between the Wilson loop and the square of the local field strength, which requires a vacuum subtraction, leading to a very poor signal-to-noise ratio. A demonstration that the fields in the region between the heavy quarks become vacuum saturated has not been realized to date.

In this work we turn to Euclidean lattice QCD in three dimensions (QCD₃), exploiting the computational advantage of this toy model (including a power law suppression of lattice discretization errors in this superrenormalizable theory) in order to convincingly demon-

strate that dynamical quarks lead to saturation of the static potential and the local color fields. This has been done using very little computational power.

Lattice studies of confinement physics using QCD₃ have a long history; this theory exhibits most of the hallmarks of four-dimensional QCD, including confinement, flux-tube formation, chiral symmetry breaking, a rich glueball spectrum, and a finite-temperature deconfining phase transition [8].

Some of the work presented here is a follow-up to an earlier study on string breaking in unquenched QCD₃ by one of us [5, 9]. What is new includes a much more extensive study of the static potential on larger lattices and with higher statistics, enabling measurements of the potential out to substantially larger R . More important, in this work we provide the first demonstration in unquenched lattice QCD, as defined in any number of dimensions, of vacuum saturation of the local color fields.

Although these results are for a three-dimensional theory, they have important implications for string breaking studies in QCD₄. In particular we find that string breaking is observed using trial states without light valence quarks, when they are propagated for Euclidean times $T \approx 1$ fm, longer than what has been attained in earlier unsuccessful studies, but not excessively so, this being the natural scale associated with hadronic binding. [As discussed in Sect. II we find a consistent relation between the physical length scales in QCD₃ and in four-dimensional hadronic physics, using two very different quantities to identify the lattice spacing in QCD₃: the quenched string tension, and the lightest unquenched vector meson mass, analogous to the ρ .]

Saturation in both the potential (as previously observed in [5]), and in the local color fields, is found to occur at separations $R \approx 1.5$ fm, which is similar to estimates of the string breaking scale in QCD₄ [10]. The correlation functions are noisy, yet a sufficiently large ensemble of configurations was generated with relatively lit-

tle computational effort, even by the standards of the intrinsically cheaper three-dimensional theory, because we used improved actions to accurately simulate on coarse lattices, with spatial spacings $a_s \approx 0.2$ fm. The same reasoning should apply to the situation in unquenched QCD₄ [6].

The rest of this paper is organized as follows. In Sect. II we describe the lattice actions and simulation parameters, and we also discuss our scale setting procedure for making contact between QCD₃ and QCD₄. Results for the static potential are presented in Sect. III and results for the local field strength in Sect. IV. A summary and some further discussion of the implications of this work for simulations of QCD₄ are found in Sect. V.

II. SIMULATIONS

Unquenched simulations of SU(2) color in three dimensions were done using a tree-level $O(a^2)$ -accurate improved gluon action, allowing for different “temporal” and “spatial” lattice spacings a_t and a_s , respectively

$$S_{imp} = -\beta \sum_{x,\mu>\nu} \xi_{\mu\nu} \left[\frac{5}{3} P_{\mu\nu} - \frac{1}{12} (R_{\mu\nu} + R_{\nu\mu}) \right], \quad (3)$$

where $P_{\mu\nu}$ is one-half the trace of the 1×1 plaquette and $R_{\mu\nu}$ is one-half the trace of the 1×2 rectangle in the $\mu \times \nu$ plane. The bare lattice anisotropy is input through $\xi_{ij} = \xi_0 \equiv (a_t/a_s)_{\text{bare}}$ [for $i, j = 1, 2$], and $\xi_{k3} = \xi_{3k} = 1/\xi_0$. The three-dimensional theory is super-renormalizable, with a bare coupling g_0^2 having dimensions of mass, and which enters Eq. (3) through the dimensionless combination $\beta = 4/(g_0^2 a_s)$.

We use the unimproved Kogut-Susskind staggered-quark action, which in three dimensions describes two flavors of four-component spinors [11]

$$S_{KS} = 2am_0 \sum_x \bar{\chi}(x)\chi(x) + \sum_{x,\mu} \zeta_\mu \eta_\mu(x) \bar{\chi}(x) [U_\mu(x)\chi(x+\hat{\mu}) - U_\mu^\dagger(x-\hat{\mu})\chi(x-\hat{\mu})], \quad (4)$$

where $\eta_\mu(x) = (-1)^{x_1+\dots+x_{\mu-1}}$ is the usual staggered phase, and where $\zeta_{1,2} = 1$, $\zeta_3 = 1/\xi_0$.

Simulations were done on a $22^2 \times 28$ lattice at $\beta = 3$, with a bare anisotropy $\xi_0 = 1/2$, and a bare quark mass $m_0/g_0^2 = 0.1$. We find that this corresponds to a rather large pion mass, with $m_\pi/m_\rho \approx 0.61$. Hence the light quark used here is actually rather heavy, comparable to the strange quark; nevertheless this quark mass is apparently light enough to resolve string breaking at accessible separations R . These parameters are very similar to those that were used in Ref. [5], although the lattice

volume is substantially larger here. For comparison the simulation parameters in the present study are compared with those in Ref. [5] in Table I.

The configurations were generated using the hybrid molecular dynamics algorithm (the Φ -algorithm) [13] with time step $\Delta t = 0.02$ and 50 molecular dynamics steps taken for each trajectory. Direct calculation of autocorrelation times for the largest Wilson loops showed $\tau \lesssim 0.2$ and, based on binning studies of autocorrelations, we elected to skip 10 trajectories between measurements. Our final data set consists of 30,000 measurements, cor-

Simulation Parameters	Ref. [5]	This work
Lattice Volume	$16^2 \times 10$	$22^2 \times 28$
β	3.0	3.0
$(a_t/a_s)_{\text{bare}}$	isotropic	1/2
m_0/g_0^2	0.075	0.10
N_{meas}	6,000	30,000

TABLE I: Comparison of simulation parameters used in an earlier study by one of us [5], and in the present work. The quenched and unquenched simulations in this work were done at the same couplings. N_{meas} is the number of measurements in each unquenched study.

responding to a total of 300,000 trajectories.

The bare parameters g_0 , m_0 , and ξ_0 are finite in the continuum limit of this super-renormalizable theory. At finite lattice spacings these parameters must absorb finite renormalizations in order to keep physical quantities fixed. However in Refs. [5, 12] it was found that little renormalization is required when the improved gluon action is employed, in the range of couplings used here. For example, the unquenched static potential showed no discernable change from $\beta = 3$ to $\beta = 2$, corresponding to a 50% increase in lattice spacing [5]; meson masses were also found to have small discretization errors [12]. Of relevance to our comparison of the quenched and unquenched results is the fact that the lattice spacings in the two theories are found to be very similar at a given bare coupling β (a quantitative comparison is made below). Moreover one finds similar meson masses in the two theories, at a given bare quark mass; for example we find $m_\pi/m_\rho \approx 0.75$ in the quenched theory, compared to the value ≈ 0.61 unquenched.

We likewise find very little renormalization of the bare lattice anisotropy. The renormalized anisotropy was determined by comparing measurements of the static potential where the direction of Euclidean time was oriented along the a_t lattice axis and then along an a_s axis. The results of the quenched simulations give a renormalized value $a_t/a_s = 0.478(7)$, while in the unquenched theory we find $a_t/a_s = 0.455(9)$ (much larger renormalizations are found if the unimproved Wilson gluon action is used [5]).

One can make rough contact between the length scales relevant to string breaking in QCD₃, and the corresponding scales in four-dimensional QCD, by identifying a confining scale in the two theories [5]. For instance, one can identify the quenched string tension in QCD₄, $\sqrt{\sigma} \approx 0.44$ GeV, with the result in quenched three-dimensional SU(2) color [8], $\sqrt{\sigma}/g_0^2 = 0.3353(18)$. In effect this allows one to express the dimensionful coupling $1/g_0^2$, or equivalently the lattice spacing a_s at a given β , in the three-dimensional theory in “fermi.” For instance at $\beta = 3$ one finds $a_s \approx 0.20$ fm. The consistency of this procedure can be established by identifying other physical quantities in QCD₃ and QCD₄. We measured the mass m_V of the lightest vector meson,

with the result $a_t m_V = 0.425(8)$ in the unquenched case, and identifying this with the physical ρ meson mass one finds $a_s \approx 0.24$ fm. In the quenched theory at the same couplings the vector meson mass is $a_t m_V = 0.380(2)$, which would identify the spacing as $a_s \approx 0.20$ fm. [This also supports the contention that the quenched and unquenched QCD₃ theories can be directly compared at the same bare couplings, though a small mismatch in the couplings will not affect the trends that we will use to establish Eqs. (1) and (2).]

It is important to note at this point that one can, and we will, establish the string breaking criteria completely within the QCD₃ theory, independent of this identification of scales with QCD₄. This connection is only used to the extent that it gives one some physical intuition for the length scales that are being probed in QCD₃, and since one may also thereby make some comparison between the parameters of the simulations that are done here, which successfully resolve string breaking, and those that have been used in various studies in QCD₄. It is to these ends that we sometimes label our simulation parameters according their values in “fermi.” We return to the comparison of our simulation results with QCD₄ in Sect. V.

III. RESULTS: STATIC POTENTIAL

We extracted the static potential from expectation values $\langle W(R, T) \rangle$ of $R \times T$ Wilson loops. Standard APE-type smearing was used for the spatial links in the Wilson loops, in order to enhance the overlap with the ground state. Measurements were done both for on-axis and many off-axis separations (i.e. using link paths joining lattice sites displaced along both spatial directions).

In order to demonstrate the onset of string breaking it is essential to carefully study the time-dependent effective potential $V(R, T)$ as a function of the propagation time T , where

$$V(R, T) \equiv -\ln \frac{\langle W(R, T) \rangle}{\langle W(R, T-1) \rangle}, \quad (5)$$

with the true ground state energy $V(R)$ given as usual by $V(R) = \lim_{T \rightarrow \infty} V(R, T)$. Results for the unquenched effective potential are presented in Fig. 1 for several values of T , and are compared with the quenched potential (the latter is evaluated at $T = 12a_t$, which is generally large enough to isolate the ground state in that case, except at the largest R ’s in the figure). The potential is also compared with the unquenched simulation determination of twice the heavy-light meson mass (using an appropriate staggered interpolating field [14]).

These results clearly demonstrate string breaking as defined by Eq. (1). An asymptote in the unquenched potential at large separations is progressively revealed as T increases; at the longest propagation time shown ($T = 12a_t \approx 1.2$ fm), the potential has clearly saturated at the expected limit of $2M_{Q\bar{q}}$ over a very wide range of

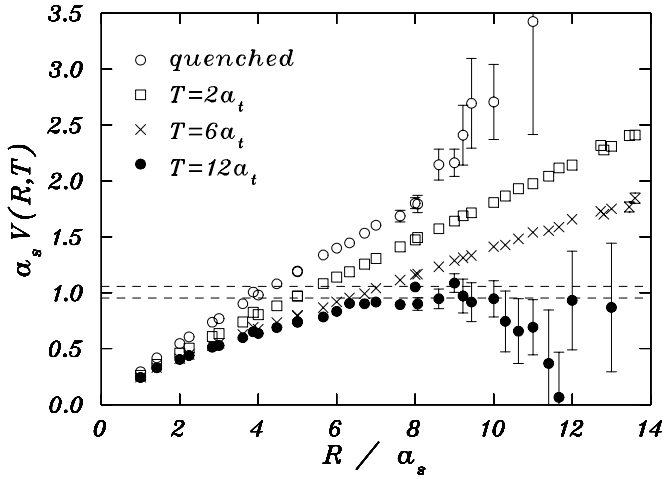


FIG. 1: Time-dependent unquenched effective potential $V(R, T)$ versus quark separation R , at several propagation times T . The quenched potential is also shown. The dashed lines give the unquenched simulation measurement of $2M_{Q\bar{q}}$.

radii. From these results one can make a rough determination of the separation R_{sb} for the onset of string breaking, corresponding to the point at which the potential reaches the correct asymptote. We find $R_{\text{sb}} \approx (6-8)a_s$. Using the scale setting procedure described in Sect. II to convert the lattice spacing to “fermi,” one obtains $R_{\text{sb}} \approx (1.2-1.6)$ fm, which is very similar to estimates of the string breaking distance in QCD₄ [10].

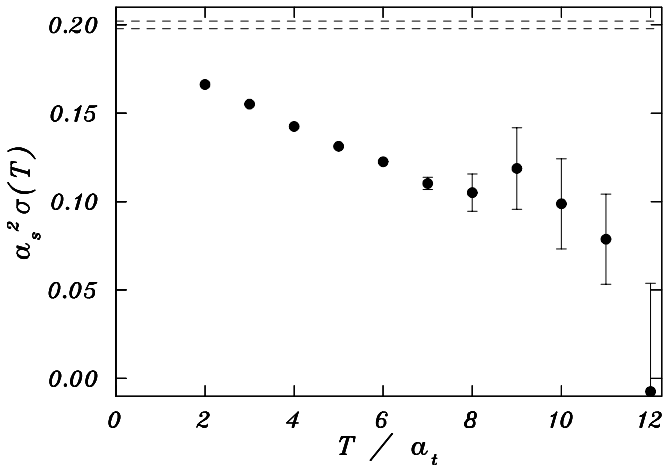


FIG. 2: Time-dependent unquenched “effective” string tension $a_s^2 \sigma(T)$, defined according to Eq. (6). The dashed lines show the quenched string tension.

To further analyze the approach to an asymptote in the effective potential as T is increased, we define an “effective” string tension $\sigma(T)$, computed from $V(R, T)$ over a small interval in separation R that is beyond the string breaking distance R_{sb} ; we take

$$V(R, T) = \sigma(T)R + b, \quad R/a_s \in [8, 10]. \quad (6)$$

Results for $\sigma(T)$ so defined were obtained from fits to the simulation measurements, and are shown in Fig. 2. The unquenched string tension clearly tends towards zero with increasing T , and this trend is manifest even at the smallest propagation times, where the measurements are most accurate. An extrapolation by-eye of the trend in $\sigma(T)$ from the smallest times would suggest that the string tension vanishes at a propagation time that is only slightly longer than what is revealed by direct inspection of an asymptote in $V(R, T)$ at large T , which clearly sets in by $T = 12a_t$, as seen in Fig. 1.

IV. RESULTS: LOCAL COLOR FIELDS

The simplest observable for measuring the local color fields comes from the correlator of a Wilson loop $W(R, T)$ with the plaquette $P_{\mu\nu}$

$$f_{\mu\nu}(\vec{x}) = -\frac{\beta}{a^3} \left[\frac{\langle W(R, T) P_{\mu\nu}(\vec{x}) \rangle}{\langle W(R, T) \rangle} - \langle P_{\mu\nu} \rangle \right], \quad (7)$$

where we suppress the dependence of $f_{\mu\nu}$ on R and T . We measure \vec{x} relative to the center of the Wilson loop. In the continuum limit (and at sufficiently large T) the above correlator corresponds to the expectation value of the square of the Euclidean field strength in the presence of the static $Q\bar{Q}$ pair, after vacuum subtraction

$$\lim_{\substack{a \rightarrow 0 \\ T \rightarrow \infty}} f_{\mu\nu}(\vec{x}) = \left\langle \text{Tr} (F_{\mu\nu}(\vec{x}))^2 \right\rangle_{Q\bar{Q}} - \left\langle \text{Tr} (F_{\mu\nu})^2 \right\rangle_{\text{vac}}, \quad (8)$$

where $F_{\mu\nu}$ denotes the usual continuum field strength, and $\langle \dots \rangle_{Q\bar{Q}}$ denotes the expectation value in the presence of the static sources, and $\langle \dots \rangle_{\text{vac}}$ is the vacuum expectation value.

The most important component of the field correlator corresponds to the color-electric field with vector component along the direction parallel to the axis joining the quark and antiquark (which, for instance, makes the largest contribution to the potential energy). We denote this correlator by $E^{\parallel}(\vec{x})$, given by

$$E^{\parallel}(\vec{x}) = -f_{1t}(\vec{x}), \quad (9)$$

where the minus sign accounts for the Euclidean contribution to the energy density, and where here the “1” direction denotes the $Q\bar{Q}$ axis and t denotes the Euclidean time axis corresponding to the small lattice spacing a_t .

We present one-dimensional profiles of the field strength, along two different lines through the flux-tube, in Figs. 3 and 4. We write $\vec{x} = (x_{\parallel}, x_{\perp})$, where x_{\parallel} is the position along the central axis joining the quarks, and x_{\perp} is the position perpendicular to that line, both measured from the center of the axis. We plot the profile along the central axis joining the quarks in Fig. 3, and along a line perpendicular to the central axis in Fig. 4. The quenched and unquenched correlators are shown in each case and, in order to emphasize the shape of the profiles in the two

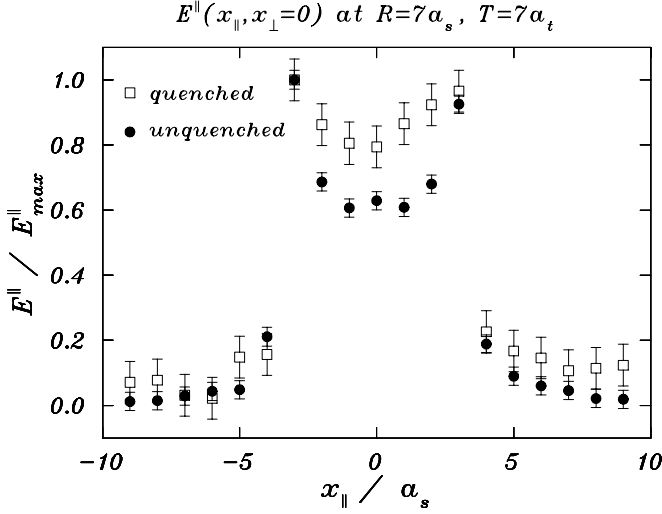
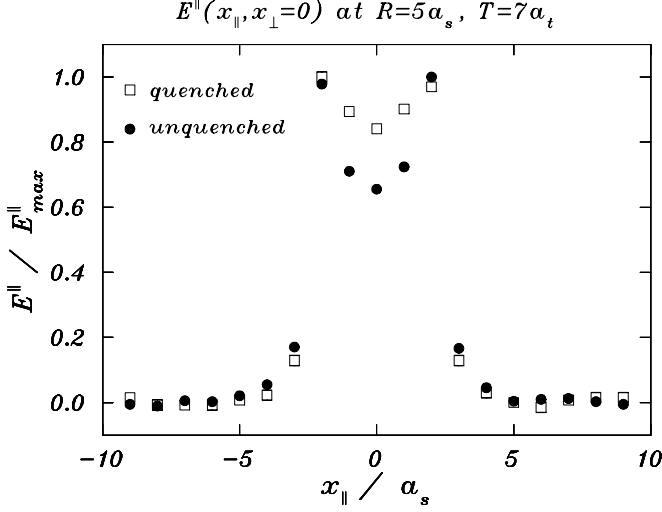


FIG. 3: Color-electric field $E^{\parallel}(x_{\parallel}, x_{\perp} = 0)$ as a function of position x_{\parallel} along the axis joining the quark and antiquark, for two values of the separation, at a fixed T . E_{\max}^{\parallel} is the maximum field strength, in the given theory, along this line (i.e. the field at the location of either quark).

theories, each correlator is normalized to its maximum value along the particular line.

The existence of a flux-tube is demonstrated in part by a “plateau” in the field strength in a region between the sources (which is expected to increase in width as R increases), where the field is approximately independent of x_{\parallel} , as seen in Fig. 3. The relative strength of the field in this region is suppressed in the unquenched theory. [We note that E^{\parallel} in the plaquette nearest to a static source, at $|x_{\parallel}| = \text{int}(R/2)$, $x_{\perp} = 0$, is generally about half as large in the unquenched theory as in the quenched case, at large R . To the extent that the couplings in the two theories are well matched, this already illustrates the suppression of the fields due to the effects of unquenching,

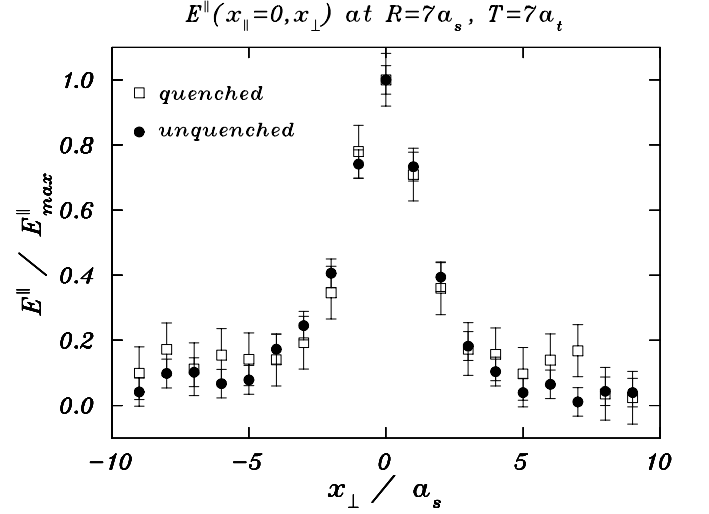
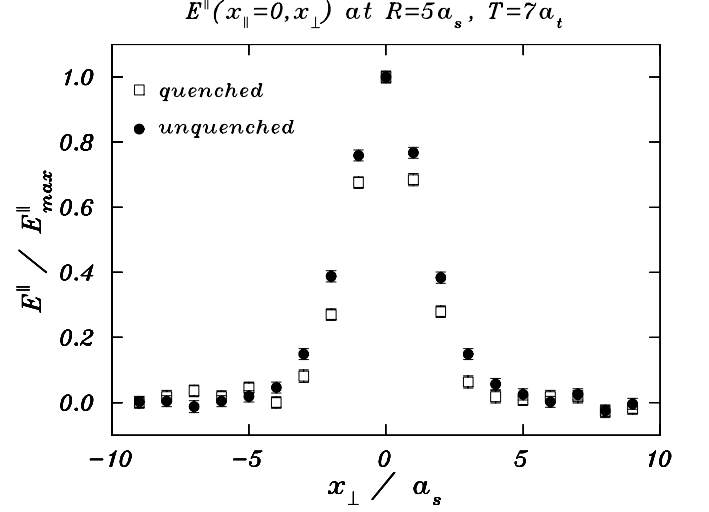


FIG. 4: Color-electric field $E^{\parallel}(x_{\parallel} = 0, x_{\perp})$ as a function of position x_{\perp} along a line perpendicular to the axis joining the quark and antiquark, for two values of the separation, at a fixed T . E_{\max}^{\parallel} is the maximum field strength, in the given theory, along this line (which in this case corresponds to the field at the midpoint of the $Q\bar{Q}$ axis).

since the correlator is an average of the squared-field over a unit cell.]

Notice as well the approximate symmetry of the flux-tube profiles about the center of the $Q\bar{Q}$ axis. The transverse widths of the flux tubes can be inferred from Fig. 4, and are indistinguishable in the unquenched and quenched cases (the width is also roughly independent of separation, which is consistent with simple models [1]).

The results in Figs. 3 and 4 are shown for fixed $T = 7a_t \approx 0.7$ fm. As indicated by the analysis of the potential in the previous section, one can easily be misled as to the extent of string breaking unless one attains propagation times of at least 1 fm. This is particularly difficult

in the case of the field correlators. Alternatively one can measure at several “intermediate” values of T , and study the systematics of increasing propagation times. To illustrate this we compare the fields at the midpoint of the $Q\bar{Q}$ axis in the two theories

$$\rho(R, T) \equiv \left[E^{\parallel}(\vec{x} = 0) \right]_{\text{unquenched}} / \left[E^{\parallel}(\vec{x} = 0) \right]_{\text{quenched}}, \quad (10)$$

where we explicitly indicate the dependence of the ratio on R and T . The results are shown in Figs. 5 and 6, which provide analogues for the fields to the effective potential plots in Figs. 1 and 2.

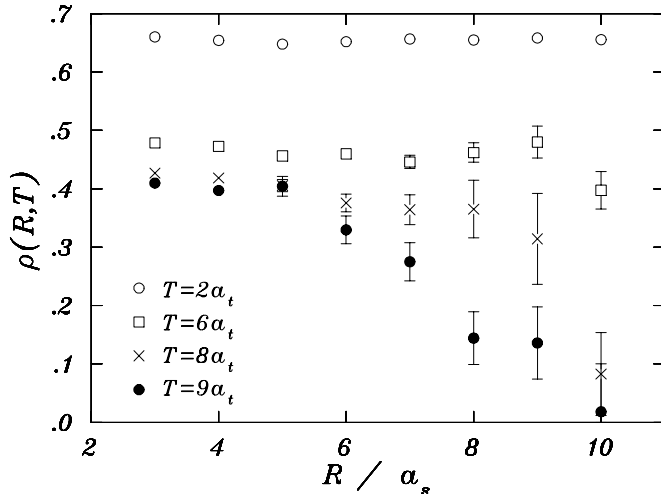


FIG. 5: Ratio of the field strengths, unquenched to quenched, at the midpoint of the $Q\bar{Q}$ axis, as a function of separation R , for various propagation times T .

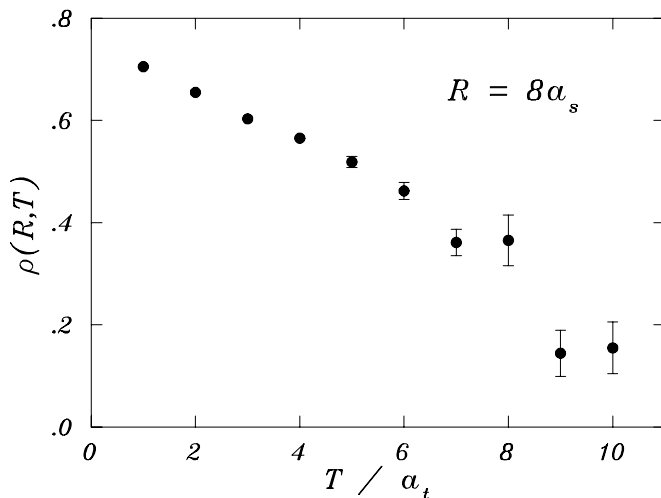


FIG. 6: Ratio of the field strengths, unquenched to quenched, at the midpoint of the $Q\bar{Q}$ axis, as a function of propagation time T , for fixed $R = 8a_s$.

The unquenched fields are suppressed at all R and T , however at modest propagation times the unquenched

field does not drop with increasing R ; taken at face value, this might suggest a failure to observe string breaking, perhaps due to some pathology in the trial states generated by Wilson loops, as has been suggested by other authors (see e.g. Refs. [7, 15]). In actuality this is simply a reflection of the fact that the ground state is not resolved unless one achieves propagation times ≈ 1 fm, which is characteristic of hadronic binding.

The systematics are particularly well illustrated in Fig. 6, which shows the time-dependence of the field strength for a fixed separation $R = 8a_s$, which was chosen because it is just beyond the string breaking distance R_{sb} . The trend is once again manifest even at small propagation times, where the signal is very clean, and an extrapolation by-eye indicates that the field becomes vacuum saturated for $T \gtrsim 12a_t$, which is consistent with our analysis of the effective potential in the previous section.

V. SUMMARY AND OUTLOOK

We were able to observe string breaking by dynamical quarks in three-dimensional QCD by working on a coarse lattice, using the staggered quark action along with an improved gluon action. String breaking was observed at large quark-antiquark separations, both as saturation of the static potential at twice the heavy-light meson mass, according to Eq. (1), and as saturation of the local field strength at vacuum values, according to Eq. (2). Measurements were done using only trial states generated by Wilson loop operators, in which no valence light quarks are present. Hence saturation of the unquenched potential and fields are highly nontrivial results, due entirely to the effects of dynamical sea quarks. The local field strength is particularly difficult to compute at the propagation times and separations at which string breaking occurs. Nonetheless computations were done over a range of propagation times that was sufficient to clearly establish the trend for the field strength to approach vacuum values in the region between the static sources.

Although this work was done in QCD₃, the results provide clear implications for large scale simulations of full QCD in four dimensions [5, 6]. Of particular importance is the need to achieve sufficiently long propagation times for the correlation functions; one can easily be misled as to the extent of string breaking unless one attains propagation times of at least 1 fm, the scale characteristic of hadronic binding. It is also sensible to work on relatively coarse lattice, using improved actions to achieve accurate results, since this alleviates the computational burden associated with generating short-distance modes that are not relevant to string breaking.

In this connection we compare the parameters of two simulations of unquenched QCD₄ (which used trial states generated only by Wilson loops) and of the present study of QCD₃, in Table II. These studies are distinguished in part by whether the string breaking condition Eq. (1) was resolved. One must exercise caution when comparing the

	QCD ₄ Ref. [15]	QCD ₄ Ref. [6]	QCD ₃ (this work)
Eq. (1)?	No	Yes	Yes
a_s	0.15 fm	0.40 fm	0.20 fm
m_π/m_ρ	0.59	0.25	0.61
T_{max}	0.4–0.8 fm	1.2 fm	1.2 fm
R_{max}	1.8 fm	1.2 fm	2.8 fm
N_{meas}	492	1,000	30,000
Volume	$16^3 \times 32$	6^4	$22^2 \times 28$

TABLE II: Comparison of some recent unquenched lattice simulations in QCD₄ and in the present QCD₃ analysis, distinguished in part by whether the particular study resolved string breaking in the static potential according to Eq. (1). The lattice spacings, meson masses, maximum quark separations R_{max} and correlation function propagation times T_{max} , number of measurements N_{meas} , and lattice volumes are compared.

two simulations in QCD₄, which were done with different actions and simulation algorithms. One must likewise exercise caution in the comparison between the QCD₄ and QCD₃ simulations (taking note of the discussion at the end of Sect. II concerning the scale setting procedure that is used for this purpose). Nonetheless this comparison is instructive, as it highlights the advantages to be gained by working on coarser lattices. In unquenched QCD₄ the

computational cost scales with lattice spacing roughly as a^{-7} , hence a small increase in the coarseness of the lattice can significantly reduce the computational cost, allowing one to generate much larger ensembles and/or to work at much smaller quark masses. Indeed the QCD₄ study in Ref. [6], which did resolve string breaking in the static potential, only required the equivalent of few PC-years of run time (comparable to the cost of the present study).

In this work we balanced the desire to use the coarsest lattice possible, in order to minimize the computational cost, against the need to have a spacing that is fine enough to resolve the spatial distribution of the color fields. We also systematically studied the trends in correlation functions with increasing propagation times, in order to leverage the cleaner data at smaller T . It is reasonable to anticipate that string breaking in the local color fields, Eq. (2), may be accessible to simulations in QCD₄, following the approach that proved successful here in QCD₃.

Acknowledgments

We thank Richard Woloshyn and Peter Lepage for helpful discussions. The work was supported in part by the Natural Sciences and Engineering Research Council of Canada.

-
- [1] See, for instance, H. D. Trottier and R. M. Woloshyn, Phys. Rev. D **48**, 2290 (1993), and references therein.
 - [2] For recent reviews see K. Kallio and H. D. Trottier, Phys. Rev. D **66**, 034503 (2002); and G. S. Bali, Phys. Rept. **343**, 1 (2001).
 - [3] Some work on zero-temperature string breaking that has appeared since the reviews in Ref. [2] include: S. Kratochvila and P. de Forcrand, Nucl. Phys. B **671**, 103 (2003); M. N. Chernodub, K. Hashimoto, and T. Suzuki, Phys. Rev. D **70**, 014506 (2004); V. G. Bornyakov et al., hep-lat/0310011.
 - [4] String breaking at finite temperature has proven to be more accessible, see e.g. C. W. Bernard et al., MILC Collaboration, Phys. Rev. D **64**, 074509 (2001).
 - [5] H. D. Trottier, Phys. Rev. D **60**, 034506 (1999).
 - [6] A. Duncan, E. Eichten and H. Thacker, Phys. Rev. D **63**, 111501 (2001); A. Duncan, E. Eichten and J. Yoo, *ibid.*, **68**, 054505 (2003).
 - [7] An alternative strategy is to use operators which generate light valence quarks in the trial state, as has been advocated in I. T. Drummond, Phys. Lett. B **434**, 92 (1998); O. Philipsen and H. Wittig, Phys. Rev. Lett. **81**, 4056 (1998); and F. Knechtli and R. Sommer, Phys. Lett. B **440**, 345 (1998). In this approach however the static potential and local color fields between the heavy quarks necessarily saturate at large R (see e.g. Kallio and Trottier, Ref. [2]); for instance such trial states exhibit saturation even in quenched simulations. Nonetheless this approach may yield useful information about the Dirac sea, not from Eqs. (1) or (2), but from measurements of mixing matrix elements between the heavy-quark trial state and the two-meson trial state.
 - [8] For a review of work on QCD₃ see M. J. Teper, Phys. Rev. D **59**, 014512 (1999).
 - [9] Some of the work in the present paper was reported in preliminary form in K. Wong, M. Sc. thesis, Simon Fraser University, 2002; and in H. D. Trottier and K. Wong, Nucl. Phys. Proc. Suppl. **119**, 673 (2003).
 - [10] C. Alexandrou *et al.*, Nucl. Phys. B **414**, 815 (1994).
 - [11] C. Burden and A. N. Burkitt, Europhys. Lett. **3**, 545 (1987).
 - [12] H. D. Trottier, Nucl. Phys. Proc. Suppl. **73**, 930 (1999). Some improvement of the three-dimensional staggered quark action was also considered in this work.
 - [13] S. Gottlieb et al., Phys. Rev. D **35**, 2531 (1987).
 - [14] A. Mihaly et al., Phys. Rev. D **55**, 3077 (1997).
 - [15] S. Aoki et al., CP-PACS Collaboration, Nucl. Phys. Proc. Suppl. **73**, 216 (1999).